Factors Affecting Nugget Growth With Mushy-Zone Phase Change During Resistance Spot Welding

P. S. Wei
Professor.
Mem. ASME

F. B. Yeh
Graduate Student.

Institute of Mechanical Engineering,
National Sun Yat-Sen University,
Kaohsiung, Taiwan

An unsteady, axisymmetric model is first proposed to investigate extensively effects of the physical, thermal, and metallurgical properties and welding conditions on nugget growths with mushy-zone phase change during resistance spot welding. The electromagnetic force, joule heat and interfacial heat generation, and cooling effects of electrodes are taken into account. Fluid patterns, temperature fields, and solute distributions in the liquid, solid, and mushy zones are determined. Results show that the computed nugget growths and temperature fields are consistent with experimental data. Variations of properties strongly affect the nugget growth. The maximum velocity in the weld nugget is found to be small and around 5 mm/s.

Introduction

Resistance spot welding has been widely used in joining workpieces. The materials to be joined are brought together under pressure by a pair of electrodes (see Fig. 1). A high electric current (usually greater than 8000 amp) passes through the workpieces between the electrodes and melts the weldments. Workpieces are thus joined as solidification of the weld pool occurs. Resistance spot welding is, therefore, a complicated process involving interactions of electrical, thermal, and metallurgical phenomena.

Heat transfer analysis is essentially required to investigate resistance spot welding. Nied (1984) proposed a highly flexible unsteady heat-conduction model and used the ANSYS finite-element computer code to determine temperature changes. The available numerical results were then applied to calculate deformation of electrodes and workpieces. Gould (1987) utilized a metallographic technique to measure weld nugget growths and developed a one-dimensional thermal model for comparison. Due to the breakdown of oxide layers and other insulating contaminants at the faying surfaces (Dickinson et al., 1980), electric contact resistance was assumed to be a linearly decreasing function of temperature. It was found that the predicted results exhibited a correct trend for the nugget development.

Wei and Ho (1990) modified the model of Gould (1987) to evaluate interfacial heat generation and joule heat. By accounting for effects of phase change, computed results showed surprisingly good agreement of the nugget thickness, nugget growth, and shape of the fusion zone with experimental data. Although the predicted nugget growths and temperatures have been achieved satisfactorily (Nied, 1984; Cho and Cho, 1989; Han et al., 1989; Wei and Ho, 1990), it is believed that the successes may be due to compensating effects of many unknown parameters, as can be seen later.

Recently, Alcini (1990) measured temperatures in the weld nugget by using beadless microthermocouples. Temperatures in the liquid nugget zone were found to be very uniform. Hence, it was concluded that strong convection occurred within the liquid nugget and the proposed swirling pattern was believed to be caused by a magnetic force. The importance of convection, however, appears to be questionable due to axisymmetry in shapes and forces for a resistance spot welding. For the sake of clarification, convection will be considered in this study.

Contributed by the Heat Transfer Division for publication in the JOURNAL OF HEAT TRANSFER. Manuscript received by the Heat Transfer Division July 27, 1990. Keywords: Materials Processing and Manufacturing Processes, Phase-Change Phenomena, Transient and Unsteady Heat Transfer.

Workpieces usually contain alloying elements. Melting or solidification of multiconstituent systems, unlike that of pure substances, is characterized by the existence of a multiphase or mushy region that separates the pure solid and liquid regions. Properties of the mushy zone control the microstructure and strength of workpieces. Savage et al. (1965) observed the microstructure and determined the conditions for occurrence of the mushy zone in resistance spot welding. A general understanding of the growth of the mushy zone as a function of the thermal, physical, and metallurgical properties and welding conditions, which are grouped by dimensionless parameters, however, has not been presented. Which factors they are and how these factors affect resistance spot welding will be investigated in this study.

In the present work, a continuum model, developed by Bennon and Incropera (1987), is used to predict the weld nugget growth by accounting for momentum, heat, and species transports in a binary solid–liquid phase-change system. A clearer understanding on resistance spot welding will be provided.

System Model and Analysis

Resistance spot welding is shown schematically in Fig. 1, as described previously. In this study, a cylindrical coordinate system is adopted to determine unsteady, axisymmetric momentum, energy, and species transport between solid, liquid and mushy zones. The major assumptions made are the following:

1 A uniform and axial electric current density is assumed for simplicity. Joule heat in the mushy zone is evaluated by using a mass-averaged electrical conductivity. Interfacial heat generation is, in fact, strongly affected by the pressure exerted by the electrodes and the surface condition of the workpieces. These factors, unfortunately, are very uncertain. A simple way to account for these factors is to introduce an effective heat transfer coefficient h_e at the contact surface between the electrode and the workpiece. Cooling effects and interfacial heat generation resulting from the workpiece–electrode contact thus can be determined. On the other hand, heat generation at the faying surface can be considered as a volumetric heat source with a small effective thickness ϵ_f (Wei and Ho, 1990). By increasing electrode pressure the effective thickness is decreased and interfacial heat becomes more concentrated. The contact resistance at ambient temperature, R_0, however, is reduced. Contact resistance also varies with temperature. In this study, contact resistance is assumed to decrease linearly

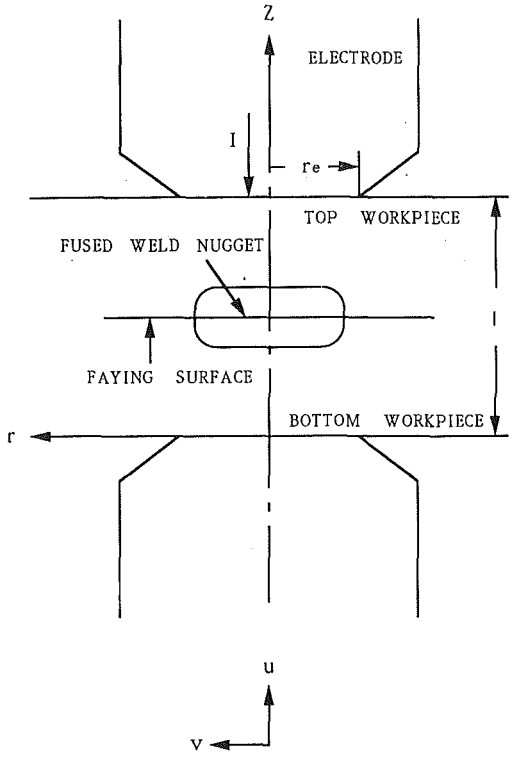

Fig. 1 Resistance spot welding process and coordinate system

with temperature to a first approximation, as suggested by Gould (1987) and Wei and Ho (1990).

2 Convection is considered. Darcy's law, which suggests that phase interaction forces are proportional to the liquid velocity relative to the velocity of the porous solid, is assumed to be applicable for modeling laminar momentum and energy transfers in the mushy zone (Ridder et al., 1981).

3 The workpieces are binary alloys. The solid and liquid in the mushy zone are assumed to be in a local thermal and phase equilibrium to a first approximation. The local equilibrium, however, does not preclude the existence of nonequilibrium conditions on a macroscopic scale (Bennon and Incropera, 1987). The solute diffusion in solid is also neglected due to a small solute diffusivity coefficient.

4 Properties of the liquid, solid, and mushy phases are assumed to be homogeneous and isotropic. Thermophysical properties are constant but different between phases.

Governing Equations. With the above assumptions, the continuity and momentum equations (Bennon and Incropera, 1987) become, respectively,

$$\frac{\partial \rho}{\partial t} + \nabla \cdot (\rho \mathbf{V}_m) = 0 \tag{1}$$

$$\frac{\partial \rho u_m}{\partial t} + \nabla \cdot (\rho \mathbf{V}_m u_m) = \mathrm{Pr} \nabla \cdot (\rho \nabla u_m) - \mathrm{Pr} \frac{\rho (1-g_l)^2}{\mathrm{Da} g_l^3} (u_m - u_s) - \frac{\partial p}{\partial z} + \mathrm{Pr}^2 \mathrm{Gr} [\theta_0 (T - T_{\mathrm{sol}}) + BF_0 (f_l^{\alpha} - f_{l, T=T_{\mathrm{sol}}}^{\alpha})] \tag{2}$$

Nomenclature

B = dimensionless parameter defined in equation (4)
$\mathbf{B}$ = magnetic flux vector, We/m^2
Bi_a, Bi_e = Biot number; $\mathrm{Bi}_a = \bar{h}_a r_e / k_s$, $\mathrm{Bi}_e = \bar{h}_e r_e / k_s$
c, C = specific heat and specific heat ratio; $C = c_l / c_s$
D = solute diffusivity, m^2/s
Da = Darcy number, defined in equation (4)
E = dimensionless electric contact resistance parameter defined in equation (10)
$\mathbf{F}$, F_r = force vector and component in r direction, N/m^3
f = mass fraction of liquid or solid
F_0 = dimensionless parameter defined in equation (4)
f^{α} = normalized solute mass fraction $= \tilde{f}^{\alpha} / \tilde{f}^{\alpha}_{m,0}$
$\tilde{f}^{\alpha}$ = solute mass fraction
$\tilde{f}^{\alpha}_{m,0}$ = initial solute content
g = volume fraction (= f for equal density between phases), or gravitational acceleration
Gr = Grashof number defined in equation (4)
h = enthalpy $= \tilde{h} / h_f$
$\bar{h}_a$, $\bar{h}_e$ = heat transfer coefficient, W/m^2-K
h_f = fusion latent heat at eutectic point, J/kg
I = welding current, amp
j = electric current density, amp/m^2
k, K = thermal conductivity and mixture thermal conductivity; $K = g_l + g_s K_h$
K_D = permeability, m^2
K_h = thermal conductivity ratio $= k_s / k_l$
k_p = equilibrium partition coefficient
K_0 = permeability constant, m^2
l, L = double workpiece thickness; $L = l / r_e$
La = dimensionless joule heat, defined in equation (4)
m = liquidus and solidus line slope parameter
p = pressure $= \tilde{p} r_e^2 / \tilde{\rho}_l \alpha_l^2$
Pr = Prandtl number
r = radial coordinate $= \tilde{r} / r_e$
R = $c_s \tilde{T}_0 / h_f$
r_e = electrode radius, m
R_f, R_0 = electrical contact resistance at any temperature and ambient temperature; $R_f = \tilde{R}_f / \tilde{R}_0$
Sc = Schmidt number
t = time $= \tilde{t} \alpha_l / r_e^2$
T, T_e = temperature and eutectic temperature; $T = \tilde{T} / \tilde{T}_0$
T_m, T_0 = melting and initial temperature
u = radial velocity $= \tilde{u} r_e / \alpha_l$
v = axial velocity $= \tilde{v} r_e / \alpha_l$
$\mathbf{V}$ = velocity vector
z = axial coordinate $= \tilde{z} / r_e$
α = thermal diffusivity, m^2/s
β_S, β_T = solutal and thermal expansion coefficient
δ_{liq}, δ_{sol} = dimensionless thickness of region surrounded by liquids and solidus line at $r = 0$
ϵ_f = effective thickness of heat source at faying surfaces, m
θ_0 = dimensionless parameter defined in equation (4)
μ_0, μ_r = free and relative magnetic permeability, N/amp^2
ν = kinematic viscosity, m^2/s
ρ = density $= \tilde{\rho} / \tilde{\rho}_l$
σ = electrical conductivity $= \tilde{\sigma} / \tilde{\sigma}_s = g_s + g_l \tilde{\sigma}_l / \tilde{\sigma}_s$
Σ = dimensionless parameter defined in equation (10)

Superscripts

α = solute
$\sim$ = dimensional quantity

Subscripts

l = liquid
liq = liquidus
m = mixture
s = solid
sol = solidus

$$\frac{\partial \rho v_m}{\partial t} + \nabla \cdot (\rho \mathbf{V}_m v_m) = \mathrm{Pr} \nabla \cdot (\rho \nabla v_m) - \mathrm{Pr} \frac{\rho (1-g_l)^2}{\mathrm{Da} g_l^3} (v_m - v_s) - \frac{\partial p}{\partial r} - La \frac{r}{2\pi^2} \quad (3)$$

where the dimensionless parameters are defined as

$$\mathrm{Pr} = \frac{\nu_l}{\alpha_l}, \quad \mathrm{Da} = \frac{K_0}{r_e^2}, \quad \mathrm{Gr} = \frac{g\beta_T (\tilde{T}_{\mathrm{sol}} - \tilde{T}_e) r_e^3}{\nu_l^2}, \quad \theta_0 = \frac{\tilde{T}_0}{\tilde{T}_{\mathrm{sol}} - \tilde{T}_e},$$
$$B = \frac{\beta_s (\hat{f}^{\alpha}_{l,e} - \hat{f}^{\alpha}_{m,0})}{\beta_T (\tilde{T}_{\mathrm{sol}} - \tilde{T}_e)}, \quad F_0 = \frac{\hat{f}^{\alpha}_{m,0}}{\hat{f}^{\alpha}_{l,e} - \hat{f}^{\alpha}_{m,0}}, \quad La = \frac{I^2 \mu_0 \mu_r}{\tilde{\rho}_l \alpha_l^2} \quad (4)$$

The second terms on the right-hand side of equations (2) and (3) are related to interactions between phases in the porous mushy zone. The isotropic permeability, according to the Kozeny–Carman equation, is

$$K_D = \frac{K_0 g_l^3}{(1-g_l)^2} \quad (5)$$

Equation (5) is generally considered valid in the laminar flow regime and applicable in this case as can be seen later. The last terms in equations (2) and (3) represent the buoyancy force resulting from the temperature and composition differences and electromagnetic force, respectively. The electromagnetic force can be found to be (Shercliff, 1965)

$$\mathbf{F} = \mathbf{j} \times \mathbf{B} \quad (6)$$

where the magnetic flux $\mathbf{B}$ can be calculated from Ampere's law

$$\nabla \times \frac{\mathbf{B}}{\mu_0 \mu_r} = \mathbf{j} \quad (7)$$

By substituting equation (7) into equation (6), the electromagnetic force becomes

$$F_r = -\frac{\mu_0 \mu_r j^2 \tilde{r}}{2} \quad (8)$$

In view of phase change in the mushy zone, the enthalpy formation for the energy equation can be conveniently used (Bennon and Incropera, 1987)

$$\frac{\partial \rho h_m}{\partial t} + \nabla \cdot (\rho \mathbf{V}_m h_m) = C \nabla \cdot (K \nabla h_m) + C \nabla \cdot [K \nabla (h_s - h_m)] - \nabla \cdot [\rho (h_l - h_m)(\mathbf{V}_m - \mathbf{V}_s)] + \frac{LaER_f}{\pi} + \frac{La\Sigma}{\sigma \pi^2} \quad (9)$$

where

$$E = \frac{\tilde{R}_0 \alpha_l}{h_f \epsilon_f \mu_0 \mu_r}, \quad \Sigma = \frac{\alpha_l}{r_e^2 h_f \tilde{\sigma}_s \mu_0 \mu_r} \quad (10)$$

and

$$h_s = RT; \quad h_l = RCT + R(1-C)T_e + 1 \quad (11)$$

The first two terms on the right-hand side of equation (9) represent the net Fourier diffusion flux; the third term is the energy flux associated with relative phase motion. The fourth term suggested by Wei and Ho (1990) is related to heat generation at the faying surface. As mentioned previously, the dimensionless electrical contact resistance at the faying surface can be expressed by

$$R_f = \frac{T_{\mathrm{liq}} - T}{T_{\mathrm{liq}} - 1} \quad (12)$$

Equation (12) indicates that contact resistance is a linearly decreasing function of temperature and it vanishes when the full-liquid weld pool occurs. The last term in equation (9) is joule heating occurring in the bulk workpieces.

The conservation requirement for species α is

$$\frac{\partial \rho f_m^{\alpha}}{\partial t} + \nabla \cdot (\rho \mathbf{V}_m f_m^{\alpha}) = \frac{\mathrm{Pr}}{\mathrm{Sc}} \nabla \cdot (\rho f_l \nabla f_m^{\alpha}) + \frac{\mathrm{Pr}}{\mathrm{Sc}} \nabla \cdot [\rho f_l \nabla (f_l^{\alpha} - f_m^{\alpha})] - \nabla \cdot [\rho (f_l^{\alpha} - f_m^{\alpha})(\mathbf{V}_m - \mathbf{V}_s)] \quad (13)$$

where the Schmidt number $\mathrm{Sc} \equiv \nu_l / D_l^{\alpha}$.

Boundary and Initial Conditions. The top workpiece surface is assumed to remain solid during the welding process

$$u_m = v_m = 0, \quad f_m^{\alpha} = 1 \qquad z = L, \quad 0 \le r < \infty \quad (14)$$

The heat loss to the top electrode is

$$-\frac{\partial h_m}{\partial z} = \mathrm{Bi}_e (h_m - R) \qquad 0 \le r \le 1 \quad (15)$$

and heat transfer loss to the surroundings is

$$-\frac{\partial h_m}{\partial z} = \mathrm{Bi}_a (h_m - R) \qquad 1 < r < \infty \quad (16)$$

Similarly, boundary conditions for the bottom workpiece are

$$u_m = v_m = 0, \quad f_m^{\alpha} = 1 \quad z = 0, \quad 0 \le r < \infty \quad (17)$$

$$\frac{\partial h_m}{\partial z} = \mathrm{Bi}_e (h_m - R) \quad 0 \le r \le 1 \quad (18)$$

$$\frac{\partial h_m}{\partial z} = \mathrm{Bi}_a (h_m - R) \quad 1 < r < \infty \quad (19)$$

The axisymmetric boundary conditions at $r = 0$ are

$$\frac{\partial u_m}{\partial r} = \frac{\partial v_m}{\partial r} = \frac{\partial f_m^{\alpha}}{\partial r} = \frac{\partial h_m}{\partial r} = 0 \qquad r = 0, \quad 0 \le z \le L \quad (20)$$

The initial temperature and temperatures of workpieces far from the weld nugget remain at the surrounding temperature $\tilde{T}_0$

$$u_m = v_m = 0, \quad f_m^{\alpha} = 1, \quad h_m = R \qquad r \to \infty, \quad 0 \le z \le L \quad (21)$$

Temperature/Enthalpy Relationships. Temperature can be determined provided that enthalpy is known. As illustrated in Fig. 2, the liquidus and solidus curves can be approximated as straight lines. Temperature versus enthalpy relationships found by Bennon and Incropera (1988) are:

1 For an enthalpy $h_m \le h_{\mathrm{sol}}$, temperature and solid fractions can be obtained to be

$$T = \frac{h_m}{R}, \quad f_s = 1 \quad (22)$$

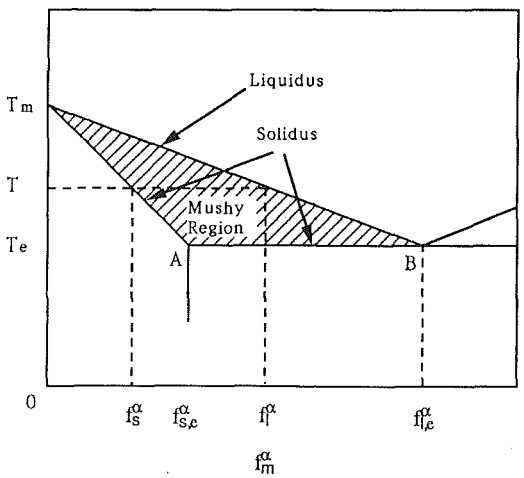

Fig. 2 Phase diagram for a binary system

where $R = c_s\bar{T}_0/h_f$ and $h_{sol} = RT_{sol}$.

2 For enthalpy $h_{sol} < h_m \leq h_e$,

$$T = T_{sol}, \quad f_s = 1 - (h_m - h_{sol}) \tag{23}$$

where

$$h_e = h_{sol} + \left[1 - \frac{1}{1-k_p}\left(\frac{T_{sol}-T_{liq}}{T_{sol}-T_m}\right)\right] \tag{24}$$

3 For enthalpy $h_e < h_m < h_{liq}$, temperature and solid fractions become

$$T^2 + \gamma_1 T + \gamma_2 = 0, \quad f_s = \frac{1}{1-k_p}\left(\frac{T-T_{liq}}{T-T_m}\right) \tag{25}$$

where

$$h_{liq} = RCT_{liq} + R(1-C)T_e + 1 \tag{26}$$

and

$$\gamma_1 = \frac{1}{1-Ck_p}\left\{(C-1)T_{liq} - k_p\left[(1-C)T_e + \frac{1}{R}\right] - CT_m(1-k_p) - \frac{1-k_p}{R}h_m\right\} \tag{27}$$

$$\gamma_2 = \frac{1}{1-Ck_p}\left\{\left[(1-C)T_e + \frac{1}{R}\right]T_{liq} - (1-k_p)T_m\left[(1-C)T_e + \frac{1}{R}\right] + \frac{1-k_p}{R}T_m h_m\right\} \tag{28}$$

4 For enthalpy $h_m > h_{liq}$,

$$T = \frac{1}{C}\left\{\frac{h_m}{R} - \left[(1-C)T_e + \frac{1}{R}\right]\right\}, \quad f_s = 0 \tag{29}$$

Supplementary Relationships. By assuming an equilibrium state in the mushy zone, the fraction of the solute α in the solid and liquid can be found to be (Bennon and Incropera, 1987)

$$f_s^\alpha = \frac{k_p f_m^\alpha}{1 + f_s(k_p - 1)} \tag{30}$$

$$f_l^\alpha = \frac{f_m^\alpha}{1 + f_s(k_p - 1)} \tag{31}$$

where the equilibrium partition coefficient k_p represents the ratio of solute contents in the solid and liquid at the same temperature. That is

$$k_p = \frac{f_s^\alpha}{f_l^\alpha} \tag{32}$$

The mean solute concentration f_m^α appearing in equations (30) and (31) at any location then can be found from equation (13).

Solution Methodology. Each of conservation equations (1)–(3), (9), and (13) can be cast in the form

$$\frac{\partial \rho\phi}{\partial t} + \nabla\cdot(\rho \mathbf{V}_m\phi) = \nabla\cdot(\Gamma_\phi \nabla\phi) + S_\phi \tag{33}$$

where a general dependent variable ϕ denotes 1, u_m, v_m, h_m, and f_m^α, respectively, and Γ_ϕ and S_ϕ are the diffusion coefficient and source term, respectively. A control-volume, staggered grid, implicit finite-difference scheme (Patankar, 1980) was used to solve the governing equations. In this work, a successive underrelaxation method was adopted with a relaxation factor of 0.5 for momentum and species, and 0.8 for pressure and temperature fields. Results were obtained by using a 42 × 53 grid in the radial and axial directions, respectively. A uniform grid spacing in the axial direction and spacing ratio of adjacent grids of 1.17 in the radial direction were chosen. A dimensionless uniform time step was chosen to be 3.5×10^{-3}. A Cyber 840A computer required around 9800 seconds, CPU time, to complete computation for 71 time steps.

The convergence criterion was met by relative errors of dimensionless velocity components less than 1×10^{-2}, enthalpy and concentration less than 1×10^{-3}. The number of iterations for dimensionless results each time is around 70. In order to compare with experimental data, 150 iterations were used. The

Table 1 Values of dimensionless parameters

Biot number, Bi_a	1.4×10^{-3}
Biot number, Bi_e	0.72
Liquid specific heat parameter, C	1.4
Darcy number, Da	1.4×10^{-5}
Electrical contact resistance parameter, E	5.6×10^{-7}
Solid-to-liquid thermal conductivity ratio, K_h	1.0
Dimensionless workpiece thickness, L	0.5
Welding current parameter, La	1.1×10^{11}
Slope parameter of liquidus line, m_{liq}	4.0
Slope parameter of solidus line, m_{sol}	3.0
Prandtl number, Pr	0.1
Solid specific heat parameter, R	0.9
Schmidt number, Sc	140
Dimensionless eutectic temperature, T_e	5.0
Dimensionless melting temperature, T_m	6.0
Thermal-to-electrical property parameter, Σ	2.0×10^{-9}
Electrical conductivity ratio, σ	1.0

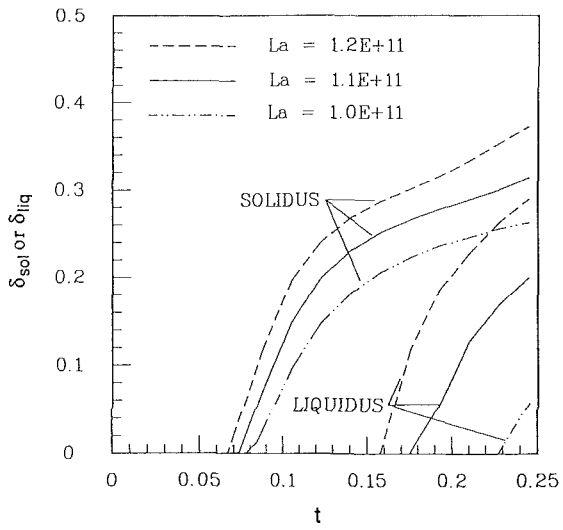

Fig. 3 Growths of the solidus and liquidus lines for different values of dimensionless welding current parameter

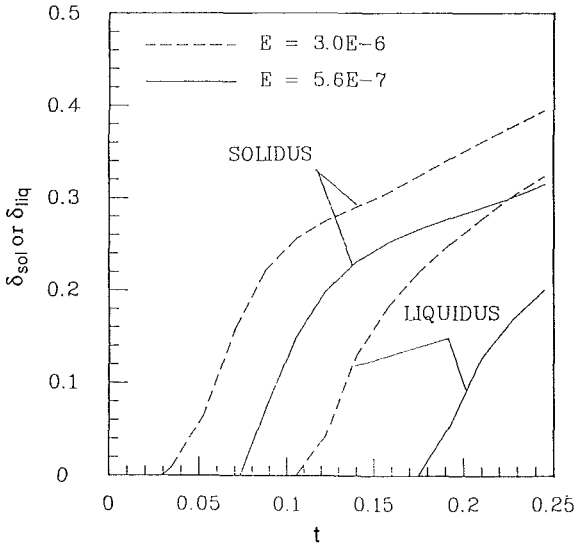

Fig. 4 Growths of the solidus and liquidus lines for different dimensionless electric contact resistances

global energy balance indicating that heat generations are balanced with the total internal energy rise and heat convected to the electrodes and surroundings is also required to assure convergence

$$\frac{\left|\int_{\nu} I^2\left(\frac{\tilde{R}_f}{\pi r_e^2 \epsilon_f}+\frac{1}{\tilde{\sigma}\pi^2 r_e^4}\right)d\nu-\int_{\nu_1}\tilde{\rho}c\frac{\partial\tilde{T}}{\partial\tilde{t}}\,d\nu_1-2\bar{h}_e\int_{A_e}(\tilde{T}_{\tilde{z}=1}-\tilde{T}_0)dA_e-2\bar{h}_a\int_{A_a}(\tilde{T}_{\tilde{z}=1}-\tilde{T}_0)dA_a\right|}{\int_{\nu} I^2\left(\frac{\tilde{R}_f}{\pi r_e^2 \epsilon_f}+\frac{1}{\tilde{\sigma}\pi^2 r_e^4}\right)d\nu} \leq 10^{-2}$$

where ν is the volume where welding current passes between electrodes, ν_1 denotes the volume of the heat-affected zone, A_e and A_a represent areas where energies dissipated to the electrode and surroundings, respectively.

Results and Discussion

In this study, resistance spot welding is found to be determined primarily by the welding current parameter $I^2\mu_0\mu_r/\tilde{\rho}_l\alpha_l^2$, dimensionless electric contact resistance $\tilde{R}_o\alpha_l/\epsilon_f h_f \mu_r\mu_0$, workpiece thickness l/r_e, Biot numbers $\bar{h}_e r_e/k_s$, solid-to-liquid thermal conductivity ratio k_s/k_l, liquid specific heat c_l/c_s, solid specific heat parameter $c_s\tilde{T}_0/h_f$, and the parameters m_{sol} and m_{liq} that are related to the slopes of the solidus and liquidus lines in the phase diagram, respectively. Values of them are chosen between pure iron and manganese to simulate a realistic resistance spot welding (Table 1).

The effect of the welding current parameter, which is related to heat generation, on the nugget growth is shown in Fig. 3. The vertical axis represents thicknesses δ_{sol} and δ_{liq} of the regions surrounded by the solidus and liquidus lines on the axisymmetric axis, respectively. For a welding current parameter $La = 1.2 \times 10^{11}$ the weld nugget or the solidus line is initiated at a dimensionless welding time of 0.0665. Thereafter, a mushy zone, that is, a mixture of solid and liquid, occurs and grows. After a welding time of 0.1575, the liquidus line appears and the weld nugget is then composed of the mushy and full-liquid regions. The thickness of the mushy zone, $(\delta_{\text{sol}} - \delta_{\text{liq}})/2$, becomes narrower as the welding time and welding current increase. This is because more energy is transferred to melt the solid. A slight increase in welding current gives rise to earlier onset, higher growth rate for both the liquid and solidus lines, and larger thicknesses of the weld nugget and full-liquid region.

As presented in Fig. 4, increasing electric contact resistance causes an early formation for both the solidus and liquidus lines, a decrease in the thickness of the mushy zone. Thickness of the weld nugget is also increased at a longer welding time.

The ratio of the workpiece thickness to electrode radius exhibits significant variations on the nugget growth and thickness, as shown in Fig. 5. Initiation times, growth rates, and movements of the solidus and liquidus lines decrease with decreasing workpiece thickness. The explanation is that the mass of a thin plate is small. Therefore, it is comparatively easy to raise temperatures in the workpieces and enhance the heat transfer rates to the electrodes (Wei and Ho, 1990).

The electrodes provide a cooling effect during the squeezing and welding cycles. Therefore, onsets of the solidus and liquidus lines are delayed, and growth rates and nugget thicknesses are reduced by increasing the Biot number, as can be seen from Fig. 6. Influence of the solid-to-liquid thermal conductivity ratio on the growth of the mushy zone is presented in Fig. 7. In view of an increase in heat transferred to melt the solid, increasing the liquid thermal conductivity results in an early formation and significant growth for both the solidus and liquidus lines. The full-liquid region does not appear in the case of the conductivity ratio above 1.25.

In view of a decrease in the energy absorbed per unit temperature rise in the liquid region and an increase of energy for melting, a low specific heat of liquid causes an early and rapid growth for both the solidus and liquidus lines, as shown in Fig. 8. Similarly, an increase in specific heat of solid delays the growth and reduces growth rate for both the solidus and liquidus lines, as presented in Fig. 9.

Characteristics of the phase diagram also have a significant influence on growths of the weld nugget and mushy zone, as shown in Fig. 10. The dimensionless parameter m_{sol} represents the ratio of the solute concentration at point A (see Fig. 2) to the initial solute content. The smaller the value of this dimensionless parameter, the steeper the solidus line is. It can be seen that decreasing the slope parameter results in an early growth for the solidus line and late formation of the liquidus

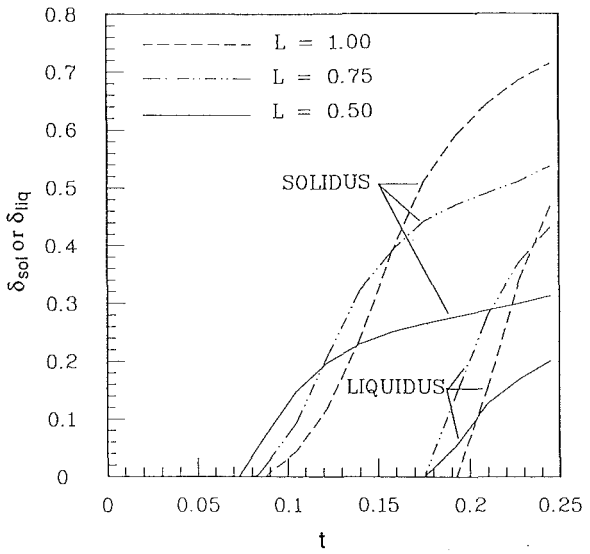

Fig. 5 Growths of the solidus and liquidus lines for different dimensionless workpiece thicknesses

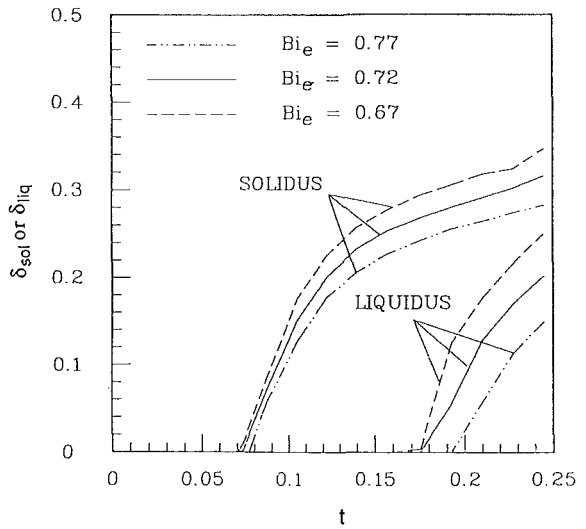

Fig. 6 Growths of the solidus and liquidus lines for different values of Biot number

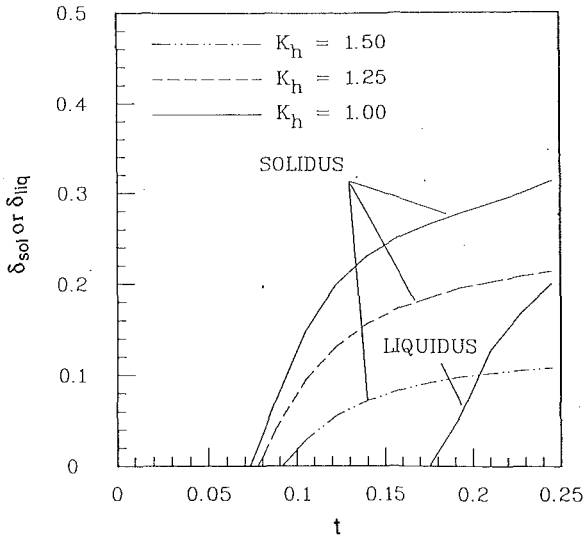

Fig. 7 Growths of the solidus and liquidus lines for different solid-to-liquid conductivity ratios

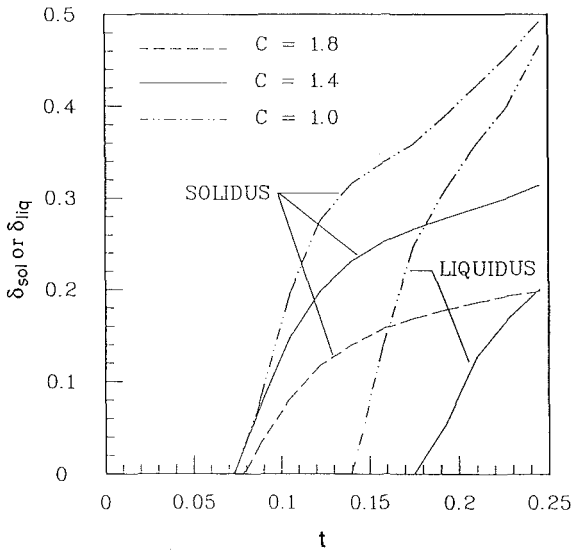

Fig. 8 Growths of the solidus and liquidus lines for different dimensionless liquid specific heats

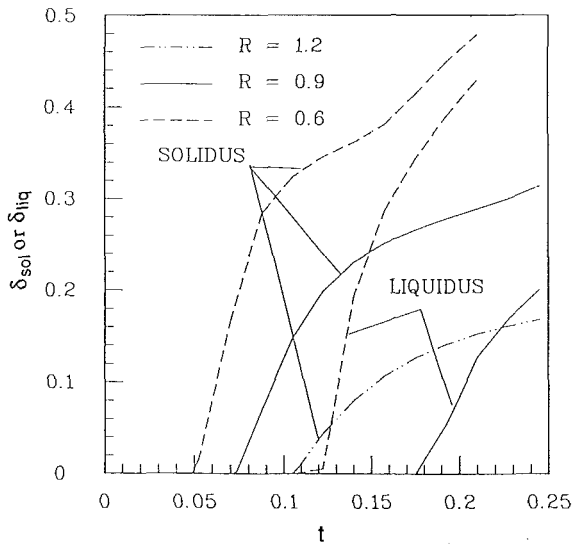

Fig. 9 Growths of the solidus and liquidus lines for different dimensionless solid specific heats

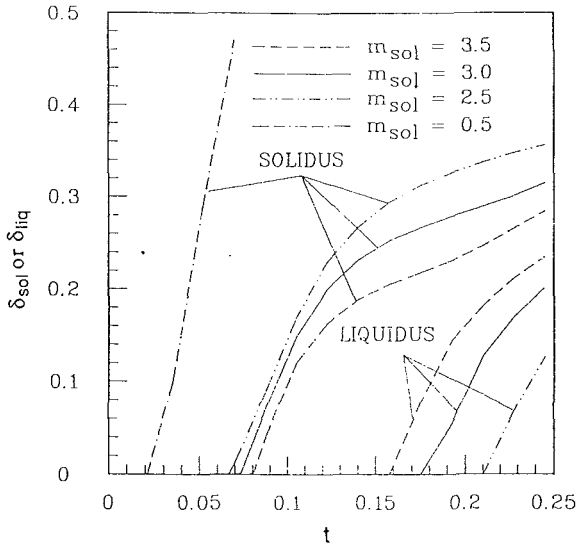

Fig. 10 Growths of the solidus and liquidus lines for different values of dimensionless slope parameter of the solidus line

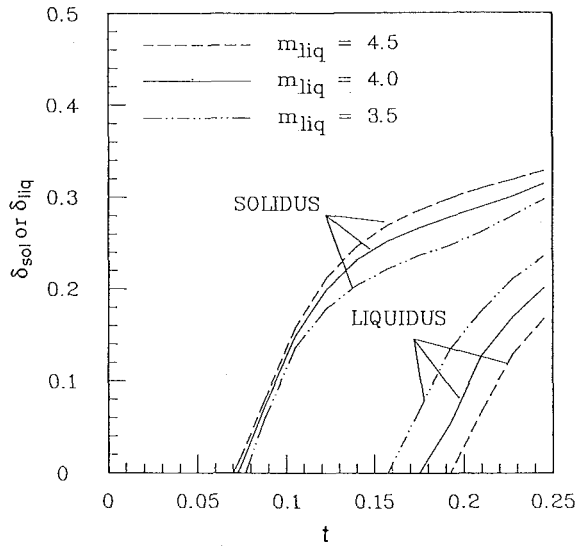

Fig. 11 Growths of the solidus and liquidus lines for different values of dimensionless slope parameter of the liquidus line

line. This is attributed to a decrease of the solidus temperature, which results in a wide range of the mushy zone and an increase of energy required for phase change (see Fig. 2). In the case of the dimensionless slope parameter equal to 0.5, the initial solute content lies between points A and B (see Fig. 2). Since the solidus temperature that corresponds to the eutectic temperature is lowest, the solidus line develops sooner.

The dimensionless parameter m_{liq} shown in Fig. 11 indicates the ratio of solute concentration at point B to the initial solute content. It can be seen that a steep liquidus line decreases the range of the mushy zone. As a result, initiation time for the liquidus line is reduced. The growth of the solidus line is found to be delayed slightly.

Referring to previous figures, it is seen that the general trend of nugget growths agrees with available experimental results for welding AISI 1008 (Gould, 1987). However, it is impossible to make an accurate comparison at the present time. The reason for this is that variations of properties have strong influence on the nugget growth, as can be seen in this study. Available data of properties such as the phase diagram with several components are also very limited. Since this study is a general

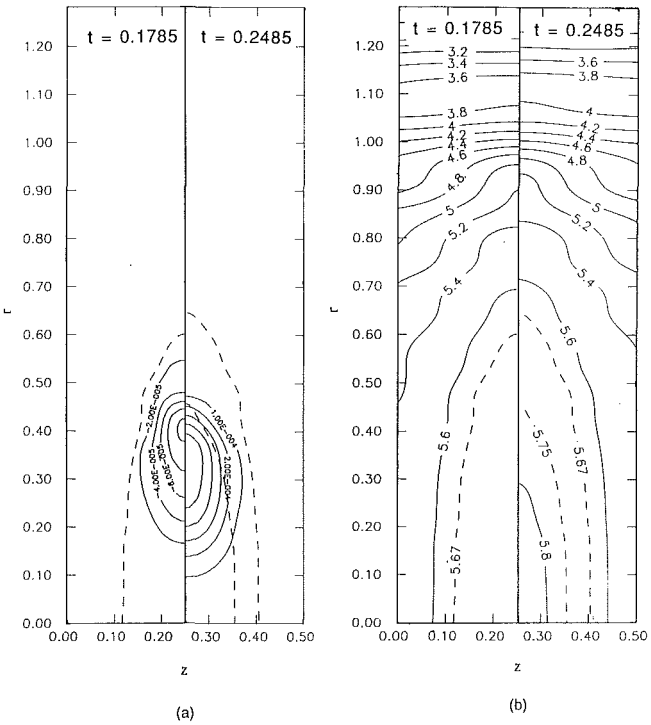

Fig. 12 *(a)* **The streamlines, and** *(b)* **isotherms at different welding times**

model that accounts for all the important factors previously indicated, the results will give a reliable and systematic insight into resistance spot welding.

The streamlines at different welding times are plotted in Fig. 12(*a*) to describe the flow pattern in the weld nugget. The dashed lines delineate the liquidus and solidus lines, respectively. It can be seen that the full-liquid region does not appear at a welding time of 0.1785. For a welding time of 0.2485 the weld nugget comprises the full-liquid and mushy regions. Motion of liquid is found to increase from the mushy zone to the full-liquid region. Liquid flows clockwise in the mushy zone due to the solute buoyancy and becomes counterclockwise in the full-liquid region as a result of thermal buoyancy. This result was qualitatively observed by Cunningham and Begeman (1965). The maximum liquid velocity was found to be around 5 mm/s, which is much smaller than the 20 cm/s and 5 m/s for the arc and high-energy beam weld pools, respectively, even though the welding current is typically 100 and 10^6 times as high. The explanation for this is that the electromagnetic force exerted on the fluid flow is nearly canceled due to axisymmetry of the resistance spot welding. Hence, fluid flow only causes a minor effect on the nugget growth and contradicts the proposition made by Alcini (1990). In the case of a radially distributed welding current density, it is noted that effects of the electromagnetic force are also small. This can be revealed by taking the curl of equation (6) and its value vanishes.

The corresponding isotherms in the solid, mushy, and liquid regions are shown in Fig. 12(*b*). It is found that the uniformity of temperatures agrees with experimental findings conducted by Alcini (1990) although convection is very small. Isotherms of 5.67 and 5.75 indicate the solidus and liquidus lines, respectively. The maximum temperature is located at the weld centerline. A significant temperature gradient occurs near the edge of electrodes ($r = 1$) and is in accord with the prediction made by Bentley et al. (1963), Wei and Ho (1990), and measurements conducted by Alcini (1990).

Since the fluid flow in the weld nugget is small, it is expected that influences of the Prandtl, Schmidt, and Darcy numbers on variations of the shape and growth of the mushy zone are insignificant and numerical computations confirm these.

Conclusions

1 Effects of the physical, thermal, and metallurgical properties and welding conditions on growths of the weld nugget and mushy zone during resistance spot welding are extensively investigated. The dimensionless parameters studied include the welding current parameter, electric contact resistance, workpiece thickness, Biot number, solid-to-liquid thermal conductivity and specific heat ratios, slopes of the solidus and liquidus lines defined in the phase diagram.

2 The solidus and liquidus lines, which define the weld nugget and mushy zone, are initiated earlier and grow more rapidly by increasing the welding current, electric contact resistance and reducing Biot number, solid-to-liquid thermal conductivity ratio, liquid and solid specific heat parameters. A steep solidus line results in an early onset of the solidus line and a late formation for the liquidus line. Increasing the slope of the liquidus line (i.e., small m_{liq}), however, causes the opposite results.

3 Convection in the weld nugget is very small. The maximum velocity is generally less than 5 mm/s even though the welding current is higher than 8000 amp.

4 Variations in the growth rate, nugget, and mushy zone thicknesses with thermal, physical, and metallurgical properties and welding conditions are pronounced. It is impossible to make an appropriate model without accounting for these factors.

References

Alcini, W. V., 1990, "Experimental Measurement of Liquid Nugget Heat Convection in Spot Welding," *Welding Journal*, Vol. 69, pp. 177-s-180-s.

Bennon, W. D., and Incropera, F. P., 1987, "A Continuum Model for Momentum, Heat and Species Transport in Binary Solid-Liquid Phase Change Systems—I. Model Formulation," *Int. J. Heat Mass Transfer*, Vol. 30, pp. 2161-2170.

Bennon, W. D., and Incropera, F. P., 1988, "Numerical Analysis of Binary Solid-Liquid Phase Change Using a Continuum Model," *Numerical Heat Transfer*, Vol. 13, pp. 277-296.

Bentley, K. P., Greenwood, J. A., Knowlson, P. Mck., and Baker, R. G., 1963, "Temperature Distributions in Spot Welds," *British Welding Journal*, Vol. 10, pp. 613-619.

Cho, H. S., and Cho, Y. J., 1989, "A Study of the Thermal Behavior in Resistance Spot Welds," *Welding Journal*, Vol. 68, pp. 236-s-244-s.

Cunningham, A., and Begeman, M. L., 1965, "A Fundamental Study of Projection Welding Using High Speed Photography," *Welding Journal*, Vol. 44, pp. 381-s-384-s.

Dickinson, D. W., Franklin, J. E., and Stanya, A., 1980, "Characterization of Spot Welding Behavior by Dynamic Electrical Parameter Monitoring," *Welding Journal*, Vol. 59, pp. 170-s-176-s.

Gould, J. F., 1987, "An Examination of Nugget Development During Spot Welding, Using Both Experimental and Analytical Techniques," *Welding Journal*, Vol. 66, pp. 1-s-10-s.

Han, Z., Orozco, J., Indacochea, J. E., and Chen, C. H., 1989, "Resistance Spot Welding: A Heat Transfer Study," *Welding Journal*, Vol. 68, pp. 363-s-371-s.

Nied, H. A., 1984, "The Finite Element Modelling of the Resistance Spot Welding Process," *Welding Journal*, Vol. 63, pp. 123-s-132-s.

Patankar, S. V., 1980, *Numerical Heat Transfer and Fluid Flow*, Hemisphere Publishing Corp., New York, Chaps. 5 and 6.

Ridder, S. D., Kou, S., and Mehrabian, R., 1981, "Effect of Fluid Flow on Macrosegregation in Axi-symmetric Ingots," *Metallurgical Transactions*, Vol. 12B, pp. 435-447.

Savage, W. F., Lundin, C. D., and Aronson, A. H., 1965, "Weld Metal Solidification Mechanics," *Welding Journal*, Vol. 44, pp. 175-s-181-s.

Shercliff, J. A., 1965, *A Textbook of Magnetohydrodynamics*, Pergamon Press, New York, p. 23.

Wei, P. S., and Ho, C. Y., 1990, "Axisymmetric Nugget Growth During Resistance Spot Welding," ASME JOURNAL OF HEAT TRANSFER, Vol. 112, pp. 309-316.